PROCEEDINGS
SPIE—The International Society for Optical Engineering

Instrumentation for Magnetospheric Imagery II

Supriya Chakrabarti
Chair/Editor

14 July 1993
San Diego, California

Volume 2008

Coded-aperture technique for magnetosphere imaging: advantages and limitations

Michael A. Gruntman

Space Sciences Center, MC-1341, University of Southern California
Los Angeles, California 90089-1341

ABSTRACT

The imaging of magnetospheres in energetic neutral atom (ENA) fluxes is recognized as a powerful experimental tool in the study of global magnetospheric processes. Intensity of ENA fluxes is typically very low, ENA's cannot be collected and concentrated by diffracting and refracting elements as it is done in optics, and therefore an imaging system on the basis of the pinhole camera should be used. There were several suggestions to use a coded-aperture technique to enhance geometrical throughput and, consequently, sensitivity of the instruments. The coded-aperture technique is reviewed and its application to the planetary magnetosphere imaging is considered. Computer simulation demonstrates advantages and limitations of the technique and promising applications are identified.

1. INTRODUCTION

The measurement of energetic neutral atom (ENA) fluxes is recognized as a powerful tool in the study of both the planetary magnetospheres and the heliosphere.[1-4] Hot magnetized plasmas in planetary magnetospheres emit magnetospheric ENA's when energetic plasma ions undergo a charge exchange interaction with background gas atoms. Conventional *in situ* measurements of magnetospheric plasma parameters cannot unambiguously distinguish between temporal and spatial variations and face difficulties in reconstructing a self-consistent global picture of magnetospheric processes. It is expected that global imaging of particle populations will substantially improve understanding of the physical processes in the planetary magnetospheres.[1,3] ENA imaging has been given a high priority in the recent NASA Space Physics Strategy-Implementation Study[5] and ENA instruments are included in scientific payloads on such missions as Cassini, Inner Magnetosphere Imager, and Imaging Super Cluster.[6]

From a remote vantage point, one could register an image of the magnetosphere in ENA fluxes. By registration of ENA images (for different atom masses and energy ranges) as they change in time, one could directly observe global magnetospheric plasma dynamics, e.g. development and decay of a ring-current during magnetic storms. Moreover, unlike other species, protons can not be imaged optically[3,7] which makes ENA's in many cases the only efficient tool to study processes of interest remotely. The powerful potential of the technique was convincingly demonstrated by Cheng[8] and Hsieh and Curtis[9] in the case of giant-planets, and by Roelof[10] and Roelof et al.[7] in the case of the Earth. In addition, populations of ENA's in interplanetary space are of interest for the study of global heliospheric processes.[2,4,11-13]

Typically ENA instrumentation requirements (see reviews by McEntire and Mitchell[14] and Hsieh et al.[15]) include a capability to identify (mass and energy) the incoming neutral particle and an imaging (direction of the particle arrival) capability. Intensity of ENA fluxes is usually very low and ENA's cannot be collected and concentrated by diffracting and refracting elements as it is done in optics. A use of coded-aperture technique for planetary magnetosphere imaging was suggested independently by Hsieh et al.[16] and Gruntman and Leonas.[17] It is believed that under certain conditions a coded aperture would allow one to enhance geometrical throughput and, consequently, sensitivity of the instruments. The goal of this work is to review the coded-aperture technique as well as specifics of its application to planetary magnetosphere imaging and to consider advantages and limitations of the technique.

At first the general requirements to ENA imaging instrumentation are discussed and the concept of aperture coding is introduced. Then the principle of operation of two-dimensional (2D) coded apertures is considered and design of the coded aperture is described. Signal-to-noise ratio of a coded-aperture system is presented and compared to that of a pinhole camera for a one-dimensional (1D) case. Computer simulation demonstrates characteristics of coded apertures and, finally, advantages and limitations of the technique are summarized and compared with the pinhole cameras.

0-8194-1257-0/93/$6.00

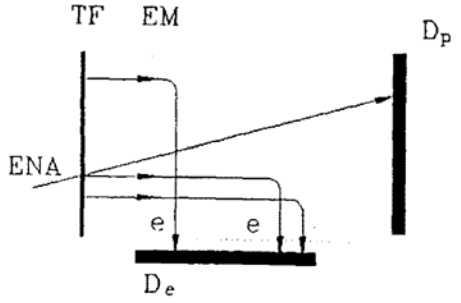

Fig.1. Generic configuration of many ENA instruments. TF - thin foil; D_e - electron detector; EM - electrostatic mirror; D_p - particle (ENA) detector.

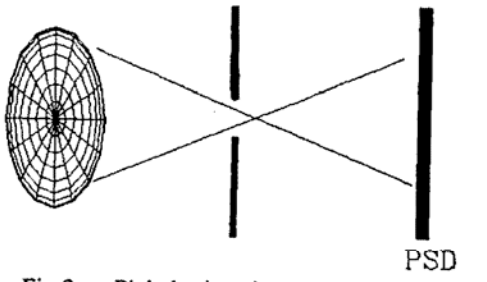

Fig.2. Pinhole imaging camera; PSD - position-sensitive detector.

2. ENA INSTRUMENT GENERIC SCHEME

Although proposed ENA instruments vary in design,[11,14,15,17,18,19] many instruments are based on the generic configuration consisting of a thin (40-1000 Å) foil, TF, followed by a particle detector, D_p (fig.1). The thin foil serves as a source of the secondary electrons emitted due to the passage of the ENA. These electrons, which are emitted from the point of foil penetration, are accelerated and directed towards a separate electron detector, D_e. The electrons can be isochronously transported to detector D_e by an electrostatic mirror[20] which allows one to accurately fix the moment of the foil penetration by the ENA and to preserve the position of the penetration point.

Detectors D_e and D_p (microchannel plate and solid-state detectors are widely used) provide START and STOP pulses, respectively, for a time-of-flight (TOF) scheme of ENA velocity measurement. A solid-state detector can be used as a detector D_p providing measurement of the ENA full energy (for ENA's with $E \geq 10$-15 keV/nucleon). Simultaneous measurement of the ENA velocity and energy is the basis for determination of the particle mass and original energy.

ENA imaging is based on a two-point trajectory extrapolation when the location of the particle entry into the instrument is connected by a straight line with the point of ENA impact on the instrument "focal plane" (where ENA image is formed). Both the particle and electron detectors can be position-sensitive (i.e. capable of determining the coordinates of the impact of each detected electron and particle), so the images formed at both the detector D_p and thin foil can be registered. Accuracy of the image transport by the electrostatic mirror to the detector D_e is mostly determined by initial energy of secondary electrons (emitted from the thin foil) and energy to which these electrons are accelerated by the voltage applied to the mirror grids. For realistic voltages, the electrostatic mirror can provide accuracy equivalent to about 30 pixels in each dimension. ENA image registration consists of reconstructing the trajectory of each detected ENA and consequently incrementing the memory cell corresponding to the reconstructed direction. Thus the image is accumulated by particle after particle registration.

When positions of both the penetration point on (electron emission from) the foil and particle impact on D_p are measured, this allows a restoration of the particle trajectory inside the instrument. For "high"-energy ENA's, this trajectory practically coincides with the direction of the particle arrival into the instrument and this direction is used for construction of an image of the ENA emitting region. For "low"-energy ENA's, the scattering in the foil becomes important and particle trajectory after the foil differs from the direction of the ENA initial velocity. Consequently, the imaging of low-energy ENA's requires the registration of the image formed by ENA's (which are unaffected by the foil) on a certain "focal" plane. In the context of imaging, the division of particles on high- and low-energy depends obviously on the foil thickness and the required angular resolution. An ENA image can be formed if the instrument entrance is limited to a small opening/hole. Therefore the imaging in the low-energy ENA fluxes requires the use of a pinhole to form the image resulting in a low instrument throughput.

Initial suggestion by Hsieh et al.[16] in 1985 to install a coded-aperture mask in front of the ENA instrument was based on the presumption that it would enhance instrument sensitivity. Independently and at the same time Gruntman and Leonas[17] proposed to use the coded-aperture technique and argued that, although the coded aperture does not have advantages over a pinhole for imaging of the magnetosphere-like objects in low-energy ENA fluxes, the coded aperture would allow one to use the *same* instrument *simultaneously* for imaging in high-energy ENA's, and for the latter, the instrument throughput would be substantially higher as compared to the pinhole camera.

One of the important elements of the instrument, which is not shown in fig.1, is a deflection system. The deflection system, which performs also the role of a collimator, is installed at the entrance of the ENA instrument to prevent (deflect) incoming charged particles (ions and electrons with $E > 100\text{-}200$ keV) from entering the sensor portion of the instrument. The simplest arrangement is to use an electrostatic deflector with a pair of parallel plates with the length, L, separation, d, and voltage between them, V.[4] The maximum energy of ions, E_{MAX}, that are deflected by such a collimator is $E_{MAX} \sim V (L/d)^2$. This dependence impose a serious limitation on the design of the imaging instrument which can be either one-dimensional or two-dimensional. A one-dimensional imaging instrument would be characterized by a much smaller separation between deflector plates, d, and consequently would allow one to achieve the desired value of E_{MAX} with much smaller values of voltage, V. From this point of view a one-dimensional imaging system seems to be much more attractive and the imaging in second dimension of the two-dimensional object can be achieved by taking advantage of the spacecraft spinning.

3. APERTURE CODING

The most straightforward way to form an image of the object in particles which cannot be controlled (by mirrors, electromagnetic fields, etc.) is to use a pinhole camera (fig.2). This is the case, for instance, for γ-rays and hard X-rays as well as for ENA's. The greater the image spatial resolution desired, the smaller the pinhole diameter should be (for the same size of the detector sensitive surface) and the speed of the image forming system may not suffice to produce an image of the desired quality during the exposure time. The situation may be aggravated by the detector noise counts that are independent of the image of the object. Such a situation is rather typical for many space experiments. To overcome the problem, the signal integration may be applied. If one produces simultaneously N images with N pinholes in the presence of the noise, for superimposed composite image the $(N)^{1/2}$ improvement of the signal-to-noise ratio may be obtained.

In the most straightforward approach, the number of not overlapping, distinct images is formed by N pinholes and these images are then added to produce the image of the object. Such a technique was successfully realized by Einighammer[21] in 1969 for as many as 85 pinholes. This approach is based, in fact, on the use of a large number of independent imaging detectors.

In another approach, the images formed by N pinholes, mix (multiplex), superimpose (not matching each other) producing the meaningless and not recognizable at first glance picture which must be unscrambled by postprocessing in order to obtain the image of the object (Fig.3). This multiplex image approach, pioneered by Dicke[22] and Ables[23] in 1968, is called the coded-aperture technique. Since then this technique was used many times in space applications, almost exclusively in X-ray astronomy, which included both the one-dimensional (e.g. by Gunson and Polychronopulos[24]) and two-dimensional imaging (e.g. by Blake et al.[25]). Many designs of the planned gamma and hard X-ray telescopes include the coded aperture masks.[26,27] It is also interesting to note that laboratory applications include multiplexing not only in space but also in time which, for example, produces spectacular results in molecular beam experiments.[28]

Although for magnetospheric application, one-dimensional imaging presents the most interest, the demonstration of the principle of operation and design of coded apertures is given for a more general two-dimensional case.

4. CODED APERTURE. PRINCIPLE OF OPERATION

The general scheme of the coded-aperture imaging instrument configuration is shown in fig.3. The object forms the multiplexed image through the mask on the sensitive surface of the recording device, e.g. position-sensitive detector. The digital image is then postprocessed to obtain the reconstructed object image. Let the two-dimensional arrays O, A, and P

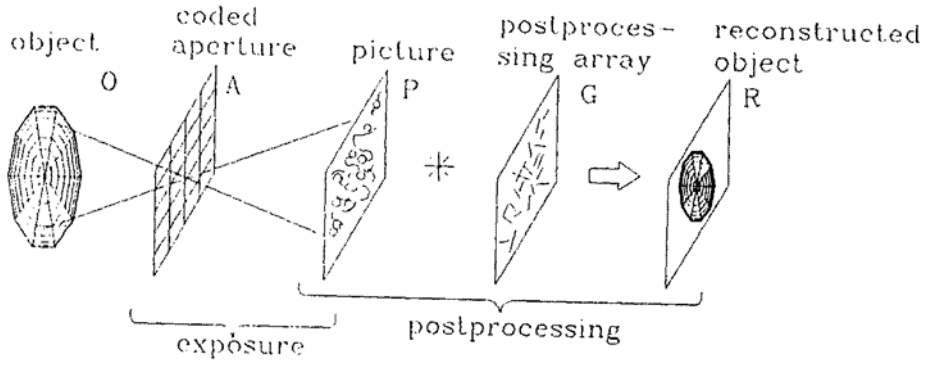

Fig.3. General scheme of the coded-aperture imaging technique

represent the object, aperture, and recorded picture, respectively. Then

$$P = O*A + N \qquad (1)$$

where N is the noise array and * denotes the correlation operator. The coded-aperture mask is the certain number of elementary (assume equal) holes in certain places and array A is correspondingly the two-dimensional binary array with elements equal to unity for hole (transmission) and to zero for the opaque material.

The use of the Fourier transform to derive O from (1) is not advantageous since small terms in the Fourier transform of A would produce a noisy reconstructed image.[29] An alternative approach[25,29,30] is to obtain the reconstructed image, R, by the convolution of P with the postprocessing two-dimensional binary array G

$$R = P*G = O*(A*G) + N*G \qquad (2)$$

If (A*G) is the δ-function, then

$$R = O + N*G \qquad (3)$$

and the reconstructed image equals the object O in the absence of the noise (N = 0). This procedure of the reconstruction of the object image is the essence of the coded-aperture imaging technique.

The quality of the imaging system can be described in terms of the point-spread function (PSF). The PSF is a reconstructed image (the system "output") of the δ-function object, and in our case, the PSF is equal to the correlation of the aperture transmission function with the postprocessing function, A*G. If the PSF is not equal to the δ-function, then the image reconstruction with the correlation postprocessing is prone to artifacts or inherent inaccuracy, as it is sometimes called. Therefore the trick is to find such an aperture and postprocessing array that their correlation is as close to the δ-function as possible.

A simple qualitative consideration may help to find the desired arrays A and G. If the distant star-like object (any object may be considered as the sum of star-like radiating sources of different intensities) illuminates the aperture mask (array A), its image (or shadow) at the detector plane will be similar to that of the mask pattern. Obviously, the correlation of this image with the mask array itself would show the central spike and sidelobes and this correlation is the autocorrelation of the array A. The ideal case would correspond to the sidelobes equal to zero. At least, they should be as flat as possible; then the image could be reconstructed by allowing for this "dc" level (pedestal) after the postprocessing procedure. Random

binary arrays, where 1's and 0's are situated randomly, would have the desired quality: due to their intrinsic randomness their sidelobes would be rather flat.

In the first applications, different types of random arrays were used for the coded-aperture design,[22-25,30] but the PSF's were not ideal. Even a computerized iterative process was tried to achieve improvements in the sidelobes shape.[25] Later, a few array types were found, for which the PSF is the δ-function or δ-function plus constant (dc) level (pedestal) depending on the particular postprocessing array, G.

One type of such arrays is the so called nonredundant arrays[31] (NRA's); their autocorrelation (A*A) consists of the central spike and sidelobes perfectly equal to unity out to some lag and either unity or zero beyond that. This means, that if one considers all possible separations between holes (i.e. 1's) in A, one finds that each separation is occurred only once, i.e. they are nonredundant. The major disadvantage of NRA's is that the ratio of the number of holes to the total number of array elements (transmission or throughput) is very low. Consequently the nonredundancy of such arrays make them ideal for the design of systems where the number of active elements (holes in our case) is to be minimized. This is the case, for instance, for the very large array configurations in radio astronomy[32].

Another class of arrays with excellent PSF and high ($\approx$0.5) transmission are the so called uniformly redundant arrays (URA's) suggested the first time for two-dimensional imaging by Fenimore and Cannon[29] in 1978. In such arrays, the number of times that a particular separation between holes (1's) occurs is constant regardless of the separation distance. Although the arrays are redundant, they are uniformly redundant. Autocorrelation for such an array would be a central spike plus the dc level.

If the uniformly redundant array A is correlated not with itself but with the array G with elements

$$\begin{aligned} G(i,j) &= 1; \quad \text{if} \quad A(i,j) = 1 \\ &= -1; \quad \text{if} \quad A(i,j) = 0 \end{aligned} \tag{4}$$

i.e. all zero elements in array A are changed to -1's to form the array G, then the PSF drastically improves. The correlation of A with G gives a perfect PSF, i.e. δ-function (more precisely δ-function multiplied by the number of the holes or 1's in the array) with zero sidelobes. The use of G in the form (4) was suggested by Brown[30] and such postprocessing was called a general mismatch scheme. For the more general case when the aperture throughput ρ differs from exactly 0.5, the perfect PSF could be obtained if elements of array G are

$$\begin{aligned} G(i,j) &= 1; \quad \text{if} \quad A(i,j) = 1 \\ &= -\rho/(1-\rho); \quad \text{if} \quad A(i,j) = 0 \end{aligned} \tag{5}$$

This technique was presented the first time by Fenimore and Cannon[29] and it is called a balanced correlation method.

The URA's seem to be an ideal choice for the aperture design for coded aperture imaging since they provide perfect PSF, high throughput and make feasible the reconstruction of the object without artifacts. One has to remember that the imperfections of the coded aperture mask manufacturing can also be a source of artifacts in the reconstructed image.[28,33,34] The questions of the signal-to-noise ratio, optimal mask transmission ρ, and tomographical capabilities of the technique were considered for URA applications in several publications.[35-37] For low intensity fluxes, even in the absence of the physical noise counts, the noise in the reconstructed object R will be present due to statistical nature of the detected flux. This form of noise is of paramount importance for the magnetospheric applications and it will be further considered in detail.

5. CODED APERTURE. DESIGN

Let us consider briefly how the URA-based two-dimensional coded-aperture pattern can be designed. The detailed description of the procedure may be found, for instance, in an article by MacWilliams and Sloane.[38] Let the dimensions of the array be $N_1 x N_2$, where N_1 is the number of rows and N_2 is the number of columns. It is necessary that the total number of URA elements $N_0 = N_1 x N_2$ can be expressed as

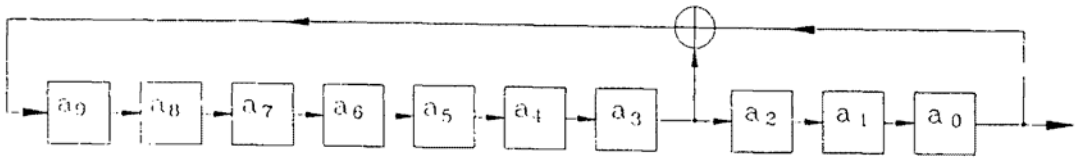

Fig.4. Linear feedback shift register corresponding to primitive polynomial $h(x) = x^{10} + x^3 + 1$. The length of the generated pseudo-random sequence is 255.

$$N_0 = 2^{k1k2} - 1 \qquad (6)$$

where URA dimensions $N_1 = 2^{k1} - 1$ and $N_2 = N_0/N_1$ are integers, relatively prime and greater than 1. We will construct here the array with $N_1xN_2 = 31x33 = 1023$ elements and $k_1 = 5$ and $k_2 = 2$.

The URA is constructed by the generation of a one-dimensional pseudo-random sequence of the length N_0 and folding (mapping) it in a proper way on a two-dimensional array. The pseudo-random sequences are widely used in communications technology and the sequence generation as well as their characteristics are described in detail by Golomb[39] and MacWilliams and Sloane.[38] A pseudo-random sequence $a_0,a_1,\ldots,a_{N0-1}$ is obtained from a primitive polynomial h(x) of degree $m = k_1 k_2$. For $m=10$ the primitive polynomial is $h(x) = x^{10} + x^3 + 1$ and the corresponding linear feedback shift register is shown in fig.4. The sign $\oplus$ denotes addition **mod 2** (EXCLUSIVE-OR gate). The nonzero initial register state is necessary, the register to be started up. Let us assume the initial state of each element of the shift register is 0 except a_9 which is equal to 1.

After the pseudo-random sequence is generated, it should be mapped on the N_1xN_2 array. The procedure of the sequence mapping is shown in fig.5, where first 200 (of 1023) sequence elements are positioned starting from the upper left corner. The upper left corner corresponds to the array-element (1,1). The direction of the mapping is shown by the solid line. Each time the sequence element is mapped, the number of the row and the number of the column are incremented by 1. While incrementing, the numbers of the row and column are considered by module N_1 and N_2 correspondingly. This means that when the number of the row (column) reaches its ultimate value $N_1(N_2)$, the next array element, where the sequence would be mapped, will have the number of row (column) equal to 1.

Figure 6 presents the resulting URA. The blackened squares correspond to 0's and white ones (holes) to 1's. The autocorrelation function of this array is a delta-function superimposed on the perfectly flat sidelobes. The height of the central spike is two times greater than that of the sidelobes. For balanced correlation, such an array provides a perfect PSF, i.e. δ-function with zero sidelobes.

6. NOISE CHARACTERISTICS

One-dimensional imaging is of the most interest for planetary magnetosphere application and noise characteristics are considered here for this case only. They can be easily extrapolated to a more general two-dimensional case.

Let us assume that we want to build an imaging system with the field-of-view covering N angular directions and no signal comes from directions outside this field-of-view (fig.7a). The angular size of the aperture element, Δ, as seen from the detector plane is equal to the angular resolution and both the detector and coded-aperture have the same size and number, N, of elements (fig.7b). For such a case only particles coming along the instrument axis would illuminate the whole detector; fluxes coming from off-axis directions would be partially blocked (fig.7b). The detector size is typically a limitation in the instrument and the dependence of the detector effective area on direction of observation is eliminated by doubling the size of the aperture and using two basic apertures sequentially (fig.7c). In the latter case, each detector element,

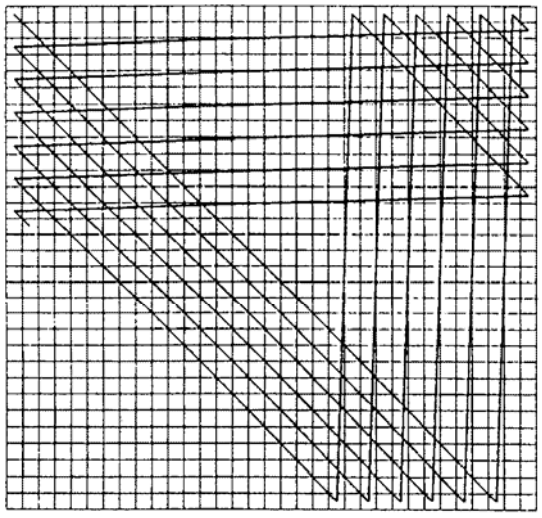

Fig.5. The sequence of the mapping 1D pseudo-random sequence on 2D array.

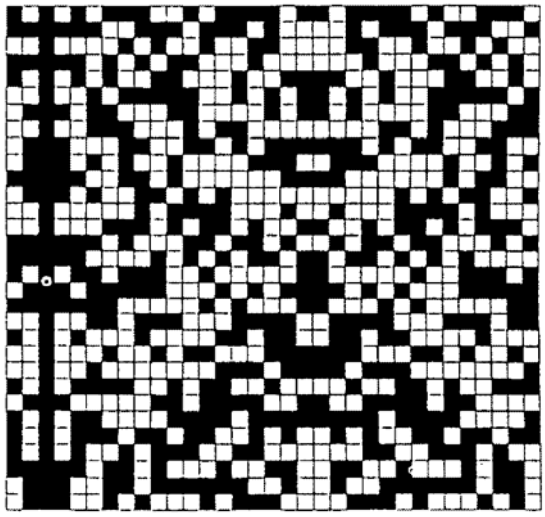

Fig.6. 2D mask based on uniformly redundant array. Blackened squares correspond to 0's and white ones (holes in the mask) to 1's.

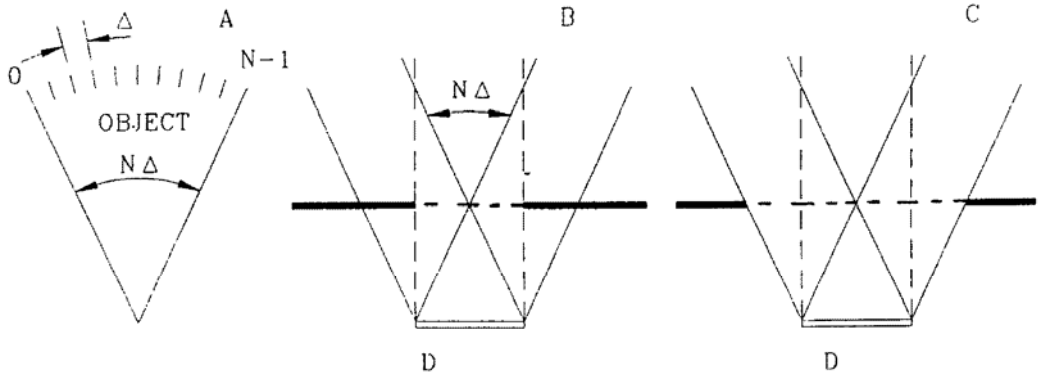

Fig.7. Coded-aperture camera with the field-of-view NΔ. A) imaging geometry; particles are coming from the directions within the field-of-view NΔ. B) imaging with the coded-aperture size equal to the size of the detector, D; effective area of the detector depends on the direction of observation. C) coded aperture is built by installing two basic sequences; effective area of the detector does not depend on the direction of the observation.

pixel, accepts the particles coming from the object through elements of exactly one basic sequence providing no particles are emitted outside the instrument field-of-view, NΔ. Particles coming from each direction within the instrument field-of-view illuminate exactly the same detector sensitive area. We will estimate the imaging noise characteristics of the code-aperture system following basically the procedure given by Comsa et al.[28]

Let us assume that

i) the object is a vector, $\bar{o}$, with elements o_i, i = 0, ...,N-1;
ii) the aperture is a binary sequence of the length 2N consisting of two consecutive basic pseudo-random sequences (a_i), i = 0, ..., N-1; number of 1's (i.e. holes) in the each sequence is n and consequently the geometrical transparency is $\rho = n/N$;
iii) the image is a vector, $\bar{p}$, with elements p_i, i = 0, ..., N-1.

Then the registered image is

$$p_k = \sum_{i=0}^{N-1} o_i \, a_{i+k} + u_k \qquad (7)$$

where the vector $\bar{u}$ (with elements u_i, i = 0, ..., N-1) is the noise counts, and $a_j = a_{j-N}$ for $2N \geq j > N$. A cyclic matrix A (size N by N) can be constructed from the basic sequence (a_i) in such a way that the first row of A is the basic sequence (a_i) and each other row is obtained from the previous one by cyclic shift of one step, i.e. $A_{ij} = a_{i+j-1}$. Then equation (7) can be rewritten as

$$\bar{p} = A\bar{o} + \bar{u} \qquad (8)$$

An image reconstruction consists of a convolution with the postprocessing array

$$G\bar{p} = (GA)\bar{o} + G\bar{u} \qquad (9)$$

where G is the postprocessing array, which is also a cyclic matrix constructed from the basic sequence (g_i) in a way similar to that of matrix A. Then if

$$GA = I \qquad (10)$$

where I is the identity matrix, the relation (9) can be rewritten as

$$o_k = \sum_{i=0}^{N-1} p_i \, g_{i+k} - \sum_{i=0}^{N-1} u_i \, g_{i+k} \qquad (11)$$

where $g_j = g_{j-N}$ for $2N \geq j > N$. For a pseudo-random sequence (a_i) the deconvolution sequence meeting requirements (10) is

$$g_i = \begin{cases} 1/n, & \text{if } a_i = 1 \\ -1/n, & \text{if } a_i = 0 \end{cases} \qquad (12)$$

and

$$\sum g_i a_{i-k} = \begin{cases} 1, & \text{if } k = 0 \\ 0, & \text{if } k \neq 0 \end{cases} \qquad (13)$$

It is important that the imaging noise can be divided into two categories. The first type is the physical noise which is independent from the object to be imaged. The vector $\bar{u}$ is such a noise and examples include detector counts induced by cosmic rays and stray electrons and photons inside the instrument. Magnetosphere imaging instruments typically require that each particle detection results in a certain sequence of pulses from detectors and certain time intervals between theses pulses (coincidences) in the instrument. Such a requirement eliminates many noise counts and in some cases ENA instruments are essentially noise-free, i.e. $\bar{u} = 0$. Another source of the noise is a statistical nature of the particle flux that forms the

image. If the number of registered particles is not high enough then the number of counts in pixels would fluctuate since the particle flux is random (Poissonian) and statistical noise is introduced herewith. The latter type of noise is present even if the physical noise is absent ($\bar{u} = 0$) and magnetosphere ENA imaging is a good example when such a noise can play the most important role.

The effect of physical noise can be easily estimated if we assume that it is uniformly distributed across the detector, i.e. $u_i = \langle u \rangle$ (notation $\langle .. \rangle$ is used for average values). Then, noting that for pseudo-random sequence

$$\sum_{i=0}^{N-1} g_i = 1/n \qquad (14)$$

one can obtain from (11)

$$o_k + \langle u \rangle / n = \sum_{i=0}^{N-1} p_i \, g_{i+k} \qquad (15)$$

One can see that the noise contribution to the restored image is a factor $1/n$ smaller in each pixel as compared to the imaging by a pinhole camera. Therefore the use of coded-aperture systems should be advantageous in the presence of the detector noise.

The variance in each accumulated pixel element, i, is equal to the number of counts there, p_i. Therefore the variance of the restored image element k is

$$\sigma^2(o_k) = \sum_{i=0}^{N-1} (g_{i+k})^2 \, (p_i + u_i) \qquad (16)$$

Noting from the equation (12) that $(g_{i+k})^2 = (1/n)^2$, one obtains

$$\sigma^2(o_k) = \frac{1}{n^2} \left[\sum_{i=0}^{N-1} p_i + N u_i \right] \qquad (17)$$

The sum in the brackets is equal to the total number of detected particles. Introducing the average signal per image element (i.e. average particle flux per an angular direction per an aperture element), $\langle o \rangle = (1/N) \sum o_i$ and noting that the total number of detected particles is a sum of the signal and noise, $\sum p_i = N n \langle o \rangle + N \langle u \rangle$, one obtains from formula (17)

$$\sigma^2(o_k) = \frac{N}{n} \left[\langle o \rangle + \frac{2 \langle U \rangle}{n} \right] \qquad (18)$$

An important feature is that the variance is uniform across the image. Therefore one can expect an improvement in imaging quality of small bright objects and somewhat worse quality of imaging of low-intensity features in the simultaneous presence of brighter parts of the object in the field-of-view. For the case of a pinhole camera, the variance of the signal accumulated during the same observation time is

$$\sigma^2(o_k) = o_k + 2 \langle u \rangle \qquad (19)$$

The gain factor, Λ, which can be defined as a ratio of the time intervals necessary to obtain the same accuracy of measurement by coded-aperture and pinhole cameras, will be given by the ratio of variances

$$\Lambda(o_k) = \frac{n}{N} \cdot \frac{o_k + 2\langle u \rangle}{\langle o \rangle + \frac{2\langle u \rangle}{n}} \qquad (20)$$

This formula allows one to determine conditions when a coded-aperture camera would provide better imaging characteristics than a pinhole camera. If $\Lambda > 1$ then the use of coded aperture technique gives advantages, if $\Lambda = 1$ then systems are equivalent, and a pinhole system is better for $\Lambda < 1$ case.

7. COMPUTER SIMULATION

7.1. Simulation scheme

We will compare imaging characteristics of a pinhole camera with a system based on a coded-aperture mask. Let us assume that the object is one-dimensional and it has 255 angular elements. The detector (and the registered image) has 255 pixels. The coded aperture consists of 510 elements, each the size of the aperture of the pinhole camera, and the coded aperture is constructed by putting together two identical basic pseudo-random sequences of the length 255 (128 holes) each. The primitive polynomial to generate such a sequence is $h(x) = x^8 + x^6 + x^5 + x^1 + 1$ (see section 5); the basic sequence is shown in fig.8. The flux of particles is assumed to be random and the number of particles that pass through an aperture element is determined by a Monte-Carlo technique in each case. The probability for a particle coming from a certain direction to hit a certain element is distributed uniformly across the coded aperture. Such a model allows the comparison of images accumulated during equal exposure (illumination) time by coded-aperture and pinhole systems.

Fig.8. The coded-aperture basic sequence generated by the primitive polynomial $h(x) = x^8 + x^6 + x^5 + x^1 + 1$.

As an example, we consider here the imaging of two extremes - a star-like object and an object with a uniformly distributed brightness. Magnetosphere images are expected to be between these two extreme cases. The effect of the object partial coding is considered as well.

7.2. Star-like object

Let us assume that there is a star-like object with intensity o_m in the instrument field of view and $o_j = 0$ for $j \neq m$. Then $\langle o \rangle = o_m/N$ and in the absence of the noise ($\langle u \rangle = 0$) the formula (20) gives us $\Lambda(o_m) = n$. Since the number of holes in the coded aperture, n, can be a rather large number, the coded aperture imaging system is far superior than the pinhole camera for imaging of star-like objects.

Figure 9 demonstrates the imaging of a star-like object (in channel 100) in the absence of noise. The object is shown in fig.9A and the image obtained by the pinhole camera is shown in fig.9B. The raw, multiplexed image recorded by the coded-aperture system and the reconstructed image are presented in fig.9C and 9D respectively. It is assumed here that the flux from the "star" is (on average) one particle per aperture element per observation (accumulation) time. The vertical scales in all four portions of the fig.9 (as well as in fig.10 and 11) are different. The number of counts in the image obtained by the pinhole camera is one. Since the particle flux is random, no particles could have been detected during this observation time. When the pinhole camera is used, then even in the absence of the detector noise one has to accumulate at least several counts (fig.9B) to be confident that this spike is the image of the object and not due to some random process. As this example shows, a coded-aperture camera is superior in sensitivity when registering star-like objects. Hence, the

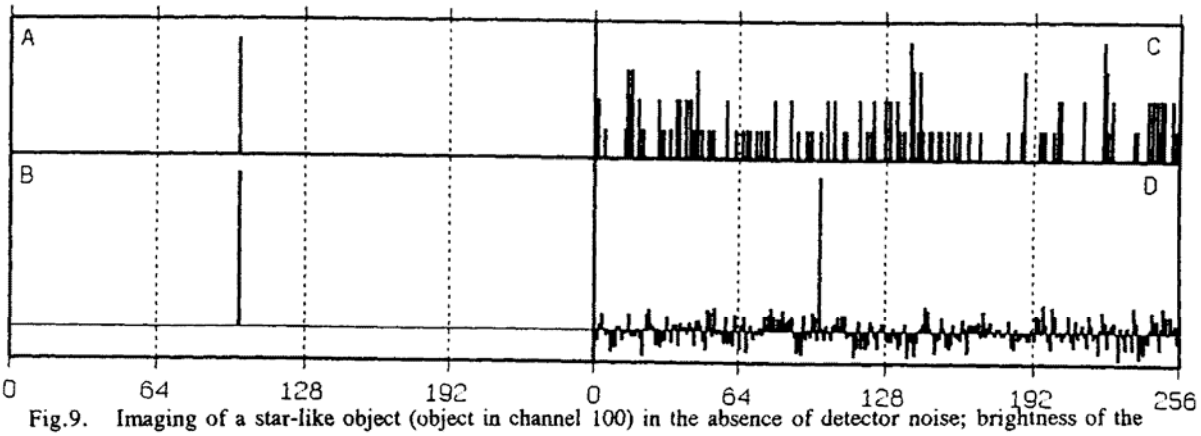

Fig.9. Imaging of a star-like object (object in channel 100) in the absence of detector noise; brightness of the object is one particle per aperture element. A - object; B - image obtained by the pinhole camera; C - raw image obtained by coded-aperture imaging system; D - reconstructed (from C) image.

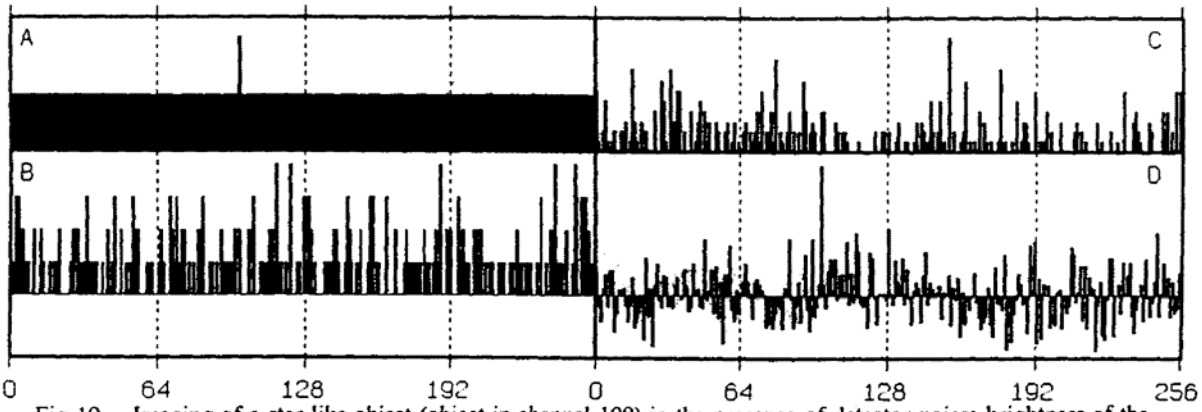

Fig.10. Imaging of a star-like object (object in channel 100) in the presence of detector noise; brightness of the object is one particle per aperture element; noise is one count per pixel. A - object; B - image obtained by the pinhole camera; C - raw image obtained by coded-aperture imaging system; D - reconstructed (from C) image.

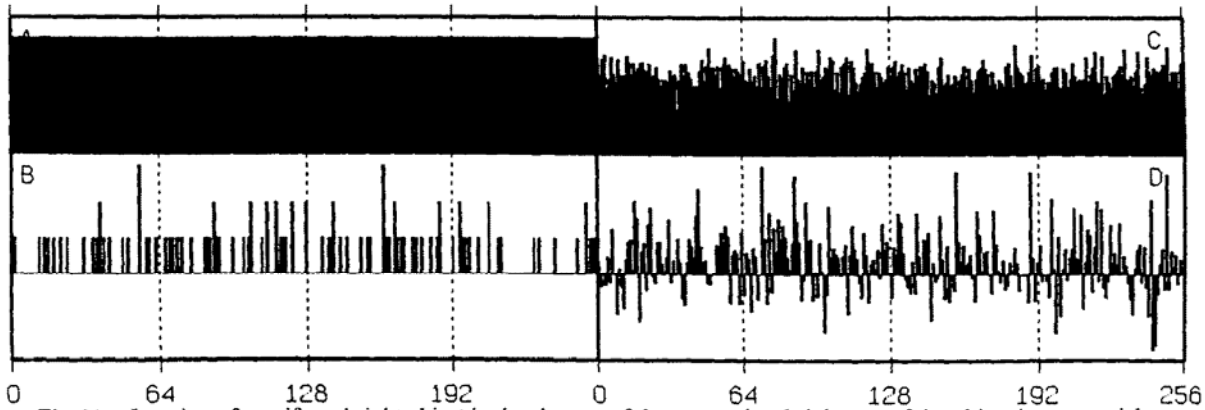

Fig.11. Imaging of a uniform bright object in the absence of detector noise; brightness of the object is one particle per aperture element per angular direction. A - object; B - image obtained by the pinhole camera; C - raw image obtained by coded-aperture imaging system; D - reconstructed (from C) image.

coded-aperture technique allows the registration of much weaker star-like objects than the objects that can be discovered by the pinhole camera.

Figure 10 demonstrates even more spectacularly the advantages of the coded-aperture camera. In this case the star-like object is accompanied by the uniformly distributed detector noise. The image corresponding to the indefinitely long accumulation time (object plus noise) is shown in fig.10A. In this example, intensities are one count per aperture element from the star and one noise count per each detector pixel. The total noise count rate of the detector is more than two orders of magnitude higher that the signal count rate. The image detected by a pinhole camera is shown in fig.10B and the star is completely "buried" in the noise. The raw image recorded by the coded-aperture system and restored image are shown in fig.10C and 10D respectively. One can clearly see that the star is definitely recognizable in the latter case.

7.3. Uniformly distributed image

Another extreme type of object is an object with uniformly distributed brightness, $o_i = <o>$. We will assume that detector noise is absent, i.e. $<u>=0$. Then, as it follows from formula (20), $\Lambda(o_m) = n/N < 1$, which means that the use of a pinhole camera is preferable over the use of a coded-aperture imaging system. The object with uniformly distributed brightness (one particle per aperture element) is shown in fig.11A. Image obtained by the pinhole camera is shown in fig.11B. The raw image obtained by the coded-aperture system is given in fig.11C, and restored image in fig.11D. The square root of variances are 0.62 and 0.87 for the pinhole and coded-aperture images respectively, being in agreement with the result of formula (20).

7.4. Partially coded objects

Until now we considered objects that are fully coded, i.e. particles are coming from the directions within the instrument field-of-view only. If part of the object is outside the instrument field-of-view, then particles coming from these directions would illuminate only part of the detector sensitive area (fig.12) resulting in image artifacts. The importance of this problem for magnetosphere imaging was emphasized by Curtis.[40] The ideal instrument performance corresponds to the object within the angular range where full image coding is achieved, i.e. where incoming particles cast a shadow

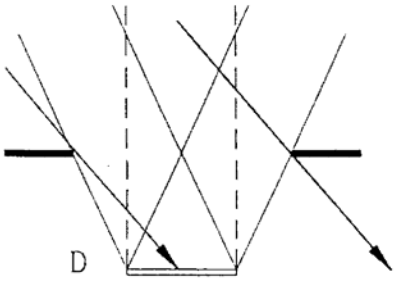

Fig.12. Partially coded imaging by a coded-aperture camera. Particles coming from ceratin directions illuminate only part of the detector sensitive area.

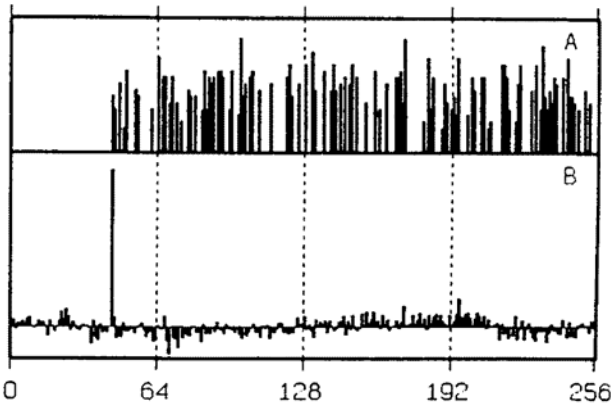

Fig.13. Example of the imaging of partially-coded objects. Object "star" is in channel 300. A - raw image by coded-aperture imaging system; B - reconstructed image.

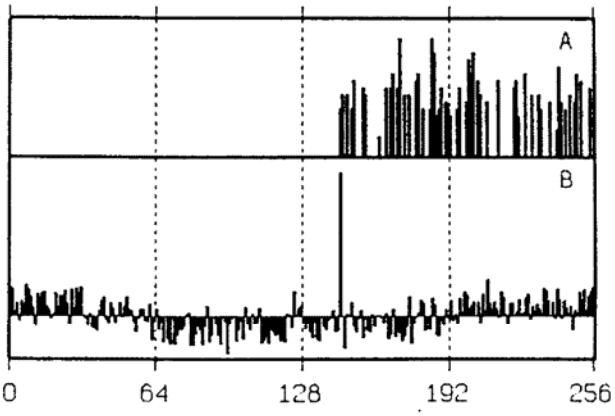

Fig.14. Example of the imaging of partially coded objects. Object "star" is in the channel 400. A - raw image by coded-aperture imaging system; B - reconstructed image.

of exactly one full basic sequence on the detector. To provide a mechanical baffle totally protecting the detector from any signal outside this field-of-view is unrealistic. Figures 13 and 14 demonstrate the effect of partial coding for a star-like source situated outside the field-of-view. The positions of the star are in channel 300 (fig.13) and channel 400 (fig.14). Star intensities are 10 particles per aperture element in each case. Figures 13A and 14A represent raw images obtained by the coded-aperture system and one can clearly see shadows corresponding to the partial coding. Figures 13 B and 14B show restored objects which are actually artifacts in channels 300-255=45 and 400-255=145 instead of channels 300 and 400 respectively. The total height of spikes is proportional to the total number of particles detected from the corresponding source. Therefore two stars of equal brightness, located outside the field-of-view, would produce two artifact spikes of unequal heights determined by the area of the detector illuminated by these two sources. It is not clear whether it is possible to eliminate artifacts due to partial coding without accurate *a priori* knowledge of the object structure outside the instrument field-of-view. At the present time the problem of partial coding represents a serious difficulty for the application of coded-aperture technique to the planetary magnetosphere imaging.

8. MAGNETOSPHERE IMAGING

Selection of the imaging system (pinhole camera or coded-aperture system) for magnetosphere imaging would depend on the specifics of the application. Several factors should be taken into account. Magnetosphere images are expected to be widely distributed (across the field-of-view) structures[3,7,10] with slowly varying brightness rather than similar to the star-like objects. For such widely distributed structures, the characteristics of the two imaging systems become comparable and in each case the decision would depend on the conditions and requirements of the experiment.

Table 1 summarizes comparison of pinhole and coded-aperture systems. We will briefly discuss all mentioned characteristics.

1. A coded-aperture camera is superior for imaging of star-like objects. This advantage becomes even more pronounced if detector noise is present.

2. The characteristics of a pinhole camera are slightly better for imaging of objects with uniformly distributed brightness. However, if detector noise is present, the coded-aperture system becomes superior.

3. The characteristics of the coded-aperture cameras are superior in the presence of the detector (physical) noise. Capability to suppress the noise is not available in pinhole cameras.

4. A pinhole camera is free from the problem of objects' partial coding. The coded-aperture technique is prone to artifacts caused by the partial coding of objects. This problem is especially important for magnetosphere imaging.

5. EUV/UV background radiation (primarily Lyman-α 1216 Å) will produce high photoelectron emission rate from the thin foil at the instrument entrance. Although electrons are rejected by the coincidence requirements, the count rate of detectors registering electrons from the foil may become too high and paralyze the instrument. Therefore the reduction of the instrument geometrical throughput may become necessary. In such conditions the use of a pinhole camera offers an advantage since the instrument effective sensitive area is much smaller than in the case of the coded-aperture camera. Consequently, the background count rate of detectors due to EUV/UV photons is much smaller for pinhole cameras.

6. The coded-aperture technique offers a unique opportunity to adjust instrument angular resolution by postprocessing. Angular resolution of the pinhole camera is fixed (we assume that no mechanically moving parts are used in instruments) and determined by the size of the pinhole itself. Coded-aperture can be formed by a large number of openings (holes) that are much smaller than the aperture of the pinhole camera. Then for bright images, the angular resolution of the coded-aperture camera would be much higher than that of the pinhole camera. When particle fluxes are small then the high-resolution image obtained by a coded-aperture camera can be digitally filtered in such a way as to produce the image of the desired statistical accuracy. Obviously, the higher the desired accuracy, the lower the angular resolution. The use of coded-aperture provides a possibility to flexibly change the angular resolution of the imaging system, varying it from image to image depending on experimental conditions and requirements. This unique feature of coded-aperture systems may be of

Table 1. Comparison of characteristics of pinhole and coded-aperture cameras.

characteristic	pinhole camera	coded-aperture camera
1. imaging of star-like objects	inferior	superior
2. imaging of objects with uniformly distributed brightness	slightly superior in the absence of noise	slightly inferior in the absence of noise
	becomes inferior with the increase of detector noise	becomes superior with the increase of detector noise
3. detector noise	problem	noise is suppressed
4. problems due to partial coding of objects	objects are fully coded	image artifacts
5. problems due to high count rates of detectors as a result of the EUV/UV background	insignificant	significant
6. electronic adjustment of the resolution	impossible	possible
7. possibility of simultaneous use for high-energy ENA imaging	no	yes
8. manufacturing imperfections	small effect	can be significant; image artifacts
9. simple/complex	simple	complex

high value for magnetosphere imaging where image brightness is expected to vary wildly. This capability is not available in pinhole cameras.

7. As it was suggested originally by Gruntman and Leonas,[17] the use of high-throughput cameras with coded apertures for low-energy ENA imaging would allow one to use them simultaneously and efficiently (i.e. with the high throughput) for the imaging in high-energy ENA's. This capability is not available in pinhole cameras.

8. Manufacturing imperfections of the pinhole aperture will not substantially affect the image quality obtained by the pinhole camera. Coded-aperture systems, on the contrary, are prone to image artifacts due to manufacturing imperfections of much more complex coded-aperture masks.

9. Pinhole cameras are much more simple in designing, building and operating than coded-aperture imaging systems.

9. ACKNOWLEDGEMENTS

The kind help of Don McMullin in preparation of this publication is highly appreciated. This work is partially supported by NASA grants NAGW-3520 and NAG 2-146.

10. REFERENCES

1. D.J.Williams, "Why we need global observations," *Magnetospheric Physics*, eds. B. Hultqvist and C.-G. Falthammer, pp.83-101, Plenum Press, New York, 1990.

2. E.C.Roelof, "Imaging heliospheric shocks using energetic neutral atoms," *Solar Wind Seven*, eds. E.Marsch and R.Schwenn, pp.385-394, Pergamon Press, 1992.

3. D.J.Williams, E.C.Roelof, and D.G.Mitchell, "Global magnetosphere imaging," *Rev. Geophys.*, Vol.30, N.3, pp.183-208, 1992.

4. K.C.Hsieh and M.A.Gruntman, "Viewing the outer heliosphere in energetic neutral atoms," *Adv. Space Res.*, Vol.13, in print, 1993.

5. Space Physics Strategy Implementation Study, A Report to the Space Physics Subcommittee of the Space Applications Advisory Committee, NASA, 1991.

6. Space Physics Missions Handbook, compiled by R.A.Cooper and D.H.Burk, Office of Space Science and Applications, NASA, 1991.

7. E.C.Roelof, B.H.Mauk, and R.R.Meier, "Instrument requirements for imaging the magnetosphere in extreme-ultraviolet and energetic neutral atoms derived from computer-simulated images," *Instrumentation for Magnetospheric Imagery*, Proc. SPIE 1744, ed. S.Chakrabarti, pp.19-30, 1992.

8. A.F.Cheng, "Energetic neutral particles from Jupiter and Saturn," *J. Geophys. Res.*, Vol.91, N.A4, pp.4524-4530, 1986.

9. K.C.Hsieh and C.C.Curtis, "A model for the spatial and energy distributions of energetic neutral atoms produced within the Saturn/Titan plasma system," *Geophys. Res. Lett.*, Vol.15, N.8, pp.772-775, 1988.

10. E.C.Roelof, "Energetic neutral atom image of a storm-time ring current," *Geophys. Res. Lett.*, Vol.14, pp.652-655, 1987.

11. M.A.Gruntman, S.Grzedzielski, and V.B.Leonas, "Neutral Solar Wind Experiment," *Physics of the Outer Heliosphere*, eds. S.Grzedzielski and D.E.Page, pp.355-358, Pergamon Press, 1990.

12. K.C.Hsieh, K.L.Shih, J.R.Jokipii, and S.Grzedzielski, "Probing the heliosphere with energetic neutral atoms," *Astrophys. J.*, Vol.393, 756-763, 1992.

13. M.A.Gruntman, "Anisotropy of the energetic neutral atom flux in the heliosphere," *Planet. Space Sci.*, Vol.40, pp.439-445, 1992.

14. R.W.McEntire and D.G.Mitchell, "Instrumentation for global magnetospheric imaging via energetic neutral atoms," *Solar System Plasma Physics*, eds. J.H.Waite Jr., J.L.Burch, and R.L.Moore, pp.69-80, AGU, Washington, DC, 1989.

15. K.C.Hsieh, C.C.Curtis, C.Y.Fan, and M.A.Gruntman, "Techniques for the remote sensing of space plasma in the heliosphere via energetic neutral atoms: a review," *Solar Wind Seven*, eds. E.Marsch and R.Schwenn, pp.357-364, Pergamon Press, 1992.

16. K.C.Hsieh, C.C.Curtis, and C.Y.Fan, *Proposal to NASA PIDDP*, 1985.

17. M.A.Gruntman and V.B.Leonas, "Possibility of experimental study of energetic neutral atoms in interplanetary space," *Proceedings, International Workshop on Problems of Physics of Neutral Particles in the Solar System*, pp.99-120, Zakopane, 1985.

18. M.A.Gruntman and V.A.Morozov, "H atom detection and energy analysis by use of thin foils and TOF technique," *J. Phys. E*, Vol.15, N.12, pp.1356-1358, 1982.

19. D.J.McComas, B.L.Barraclough, R.C.Elphic, H.O.Funsten III, and M.F.Tomsen, "Magnetospheric imaging with low-energy neutral atoms," *Proc. Nat. Acad. Sci. U.S.A.*, Vol.88, pp.9598-9602, 1991.

20. F.Busch, W.Pfeffer, B.Kohlmeyer, D.Schull, and F.Puhlhoffer, "A position-sensitive transmission time detector," *Nucl. Instrum. Methods*, Vol.171, pp.71-74, 1980.

21. H.J.Einighammer, "Detection of weak X-ray sources by image integration," *Vth Intern. Congress on X-ray Optics and Microanalysis*, eds. G.Moellenstedt and K.H.Glauker, pp.50-54, Springer, 1969.

22. R.H.Dicke, "Scatter-hole cameras for X-rays and gamma rays," *Astrophys. J. Lett.*, Vol.153, pp.L101-L106, 1968.

23. J.G.Ables, "Fourier transform photography: a new method for X-ray astronomy," *Proc. Astron. Soc. Australia*, Vol.1, N.4, pp.172-173, 1968.

24. J.Gunson and B.Polychronopulos, "Optimum design of a coded mask X-ray telescope for rocket applications," *Mon. Not. R. Astron. Soc.*, Vol.177, pp.485-497, 1976.

25. R.L.Blake, A.J. Burek, E.E. Fenimore, and R.Puetter, "Solar X-ray photography with multiplex pin-hole camera," *Rev. Sci. Instrum.*, Vol.45, pp.513-516, 1974.

26. G.Boella, A.Bussini, R.C.Butler et al., "The basic unit of the imaging plane of the ZEBRA low energy gamma ray telescope," *IEEE Trans. Nucl. Sci.*, Vol.NS-33, N.1, pp.755-758, 1986.

27. J.E.Grindlay, M.R.Garcia, R.L.Burg, and S.S.Murray, "The energetic X-ray imaging telescope experiment (EXITE)," *IEEE Trans. Nucl. Sci.*, Vol.NS-33, N.1, pp.750-754, 1986.

28. G.Comsa, R. David, and B.J.Schumacher, "Magnetically suspended cross-correlation chopper in molecular beam-surface experiments," *Rev. Sci. Instrum.*, Vol.52, N.6, pp.789-796, 1981.

29. E.E.Fenimore and T.M.Cannon, "Coded aperture imaging with uniformly redundant arrays," *Appl. Opt.*, Vol.17, N.3, pp.337-347, 1978.

30. C.Brown, "Multiplex imaging with multiple-pinhole cameras," *J. Appl. Phys.*, Vol.45, N.4, pp.1806-1811, 1974.

31. M.J.E.Golay, "Point arrays having compact, nonredundant autocorrelations," *J. Opt. Soc. Am.*, Vol.61, N.2, pp.272-273, 1971.

32. W.K.Klemperer, "Very large array configurations for the observation of rapid varying sources," *Astron. Astrophys. Suppl.*, Vol.15, N.3, pp.449-451, 1974.

33. M.H.Tai, M.Harwit, and N.L.A.Sloane, "Errors in Hadamard spectroscopy or imaging caused by imperfect masks," *Appl. Opt.*, Vol.14, N.11, pp.2678-2686, 1975.

34. N.J.A.Sloane, M.Harwit, and M.-H.Tai, "Systematic errors in Hadamard transform optics," *Appl. Opt.*, Vol.17, N.18, pp.2991-3002, 1978.

35. E.E.Fenimore, "Coded aperture imaging: predicted performance of uniformly redundant arrays," *Appl. Opt.*, Vol.17, N.22, pp.3562-3570, 1978.

36. T.M.Cannon and E.E.Fenimore, "Tomographical imaging using uniformly redundant arrays," *Appl. Opt.*, Vol.18, N.7, pp.1052-1057, 1979.

37. S.R.Gottesman and E.J.Schneid, "PNP - a new class of coded aperture arrays," *IEEE Trans. Nucl. Sci.*, Vol.NS-33, N.1, pp.745-749, 1986.

38. F.J.MacWilliams and N.J.A.Sloane, "Pseudo-random sequences and arrays," *Proc. IEEE*, Vol.64, N.12, pp.1715-1729, 1976.

39. S.W.Golomb, *Digital Communications with Space applications*, Prentice Hall Inc., Englewood Cliffs, N.J., 1964.

40. C.C.Curtis, "Aperture codes for sensors viewing extended objects from space," *Instrumentation for Magnetospheric Imagery*, SPIE 1744, ed. S.Chakrabarti, pp.161-170, 1992.